International Journal of Bifurcation and Chaos, Vol. 4, No. 4 (1994) 823–841

Papers

[P16]

CONSTRUCTING HOMOCLINIC ORBITS AND CHAOTIC ATTRACTORS

BO DENG
Department of Mathematics and Statistics, University of Nebraska Lincoln, Lincoln, NE 68588, USA

Received July 9, 1993; Revised February 20, 1994

Homoclinic orbits and chaotic attractors are constructed progressively by singular perturbations. More specifically, lower dimensional slow subsystems and fast subsystems are constructed separately as building blocks. The former are then modulated onto the latter via homotopy. This gives a systematic way to implement Rössler's dual principle for mathematical modeling. Systems constructed in this way are simple, robust, and ideal for the purposes of experimental and theoretical analyses.

1. Introduction

An important stage in mathematical modeling occurs when a set of equations is written down according to certain idealized physical laws. It is usually not feasible, if not altogether impossible, to take into account all the properties of the system. A further mathematical idealization thus follows. The latter process is very much apparent in the normal form theory in which normal forms are derived from real systems yet stripped of all physical meanings. Studies on the normal forms have contributed a great deal to our understanding on nonlinear structures of dynamical systems.

There is little difficulty involved in writing down a normal form for, say, the Hopf bifurcation. However, it is a completely different matter to write down a system having a homoclinic orbit to a Shil'nikov's saddle-focus equilibrium point, or a homoclinic orbit whose unstable manifold twists like the Möbius band, or a system having an attracting strange toroid. Most important of all, if such a phenomenological modeling is indeed possible, what is the guiding principle behind it, if any? An answer to this question will undoubtedly shed some light on how natural systems build themselves and provide us with a greater degree of freedom in choosing simpler models for future experimental and theoretical investigations.

It turns out that an answer to this question lies in a practicable version of the so-called dual principle first postulated by Rössler in 1976. It was stated in Rössler [1976] that "(each of his artificially constructed systems) consists of (1) an ordinary two-variable chemical oscillator and (2) an ordinary single-variable chemical hysteresis system." He also went on by claiming that "according to the same dual principle, many more analogous systems can be devised, no matter whether chemical, biochemical, biophysical, ecological, sociological, economic, or electronic in nature." For implementation of his dual principle, he suggested a trail-and-error process as he wrote "..., the described system is just one out of a huge variety of possible combinations of an oscillator, on the one hand, and a switching system, on the other." However impractical, his approach has delivered a few unexpectedly, including the Rössler attractor; see Rössler [1976,1979].

The purpose of this paper is to describe a systematic method to implement the Rössler dual principle. It has two key components, one deals with

the construction of the switching, or fast subsystem $\varepsilon\dot{z} = h(x, y, z, \varepsilon)$ and the other the oscillator, or the slow subsystem $\dot{x} = f(x, y, z, \varepsilon), \dot{y} = g(x, y, z, \varepsilon)$. The resulting system is in this singularly perturbed form $\dot{x} = f(x, y, z, \varepsilon), \dot{y} = g(x, y, z, \varepsilon), \varepsilon\dot{z} = h(x, y, z, \varepsilon)$.

Roughly speaking, our method calls for the following forms for functions f, g, h. For $\varepsilon = 0$, $h(x, y, z, 0) = (z - z_1)(z - z_2)p(x, y, z)$ and $\mathbf{f}(x, y, z, 0) = (z - z_1)\mathbf{f}_1(x, y) + (z - z_2)\mathbf{f}_2(x, y)$, where z_1, z_2 are constants, $p, \mathbf{f}_1, \mathbf{f}_2$ are some carefully chosen polynomials with $\mathbf{f} = (f, g), \mathbf{f}_1 = (f_1, g_1), \mathbf{f}_2 = (f_2, g_2)$. Thus, $z = z_1, z_2$ are two branches of the slow manifold and the reduced slow subsystem is $\dot{x} = (z_1 - z_2)f_2(x, y), \dot{y} = (z_1 - z_2)g_2(x, y)$ on $z = z_1$ and $\dot{x} = (z_2 - z_1)f_1(x, y), \dot{y} = (z_2 - z_1)g_1(x, y)$ on $z = z_2$ respectively. The properties of this type of singular perturbations that are critical to our method include:

(1) By choosing the factor p accordingly, one can construct a hysteresis so that those parts of $z = z_1, z_2$ that are contained in the hysteresis are asymptotically attracting.

(2) Because orbits from certain region containing the hysteresis stay in a small neighborhood of these attracting branches of the planes most of the time, the dynamics in that region is completely determined by our choices of $\mathbf{f}_1, \mathbf{f}_2$. Thus, the virtually unlimited combinations in choosing $p, \mathbf{f}_1, \mathbf{f}_2$ enable us to construct models according to our specifications. This is what we want to demonstrate in this paper. Examples are organized according to the types of hysteresses, which we will refer to as switches from now on.

2. Simple Switches

2.1. *Shil'nikov's saddle-focus homoclinic orbit*

A system having such an orbit satisfies the condition that there is a homoclinic orbit of a saddle-focus equilibrium point at which the linearization of the vector field has eigenvalues $\lambda \pm i\omega, \mu$,

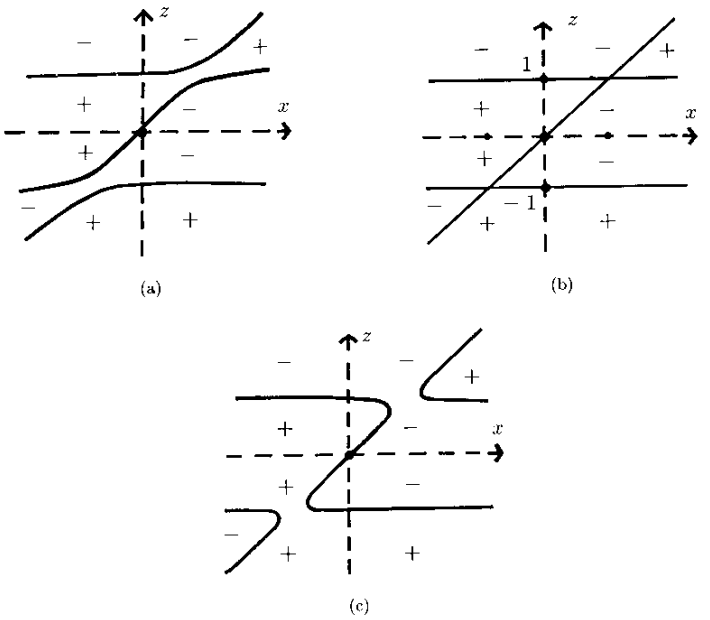

Fig. 1. The construction of a Z-switch. $\pm$ are the sign for the fast component $\dot{z}$ in the regions partitioned by the nullclines for (a) $\varepsilon < 0$, (b) $\varepsilon = 0$, (c) $\varepsilon > 0$.

satisfying $0 < \lambda < -\mu$, $\omega \neq 0$, see [Shil'nikov, 1970]. Our model system is

$$\begin{aligned}
\dot{x} &= -(z+2)d(x-a) + (2-z) \\
&\quad \times \left[\alpha(x-2) - \beta y - \alpha(x-2)\frac{(x-2)^2+y^2}{R^2}\right], \\
\dot{y} &= -(z+2)(y-b) + (2-z) \\
&\quad \times \left[\beta(x-2) + \alpha y - \alpha y\frac{(x-2)^2+y^2}{R^2}\right], \\
\varepsilon\dot{z} &= (4-z^2)[z+2-m(x+2)] - \varepsilon c z\,,
\end{aligned} \tag{1}$$

where a, b, c, d, m, R, α, β are parameters and ε the singular parameter.

For the switching subsystem, the nullcline consists of the roots of the cubic polynomial $h(x, y, z, \varepsilon) = (4-z^2)[z+2-m(x+2)] - \varepsilon c z$ in z. At $\varepsilon = 0$, $z = \pm 2$ and $z + 2 - m(x+2) = 0$ for $h(x, y, z, 0) = 0$. For $0 < \varepsilon \ll 1$, the two intersection points $x = z = -2$ and $x = 4/m - 2$, $z = 2$ of the three planes bifurcate into four turning points due to the fact that h is a cubic polynomial. By the continuity in $0 < \varepsilon \ll 1$, the rest of the planes remains almost unchanged. That is, the nullcline rearranges itself into three connected components and a Z-shaped hysteresis emerges in the middle as depicted in Fig. 1(c). Moreover, when treating the x, y variables as parameters, the two horizontal planes $z = \pm 2$ consist of attracting equilibrium points of the fast subsystem. We will call such a hysteresis curve a Z-switch. We remark that this technique was used in Rössler [1979] and we will use it in this paper to construct all fast switching subsystems.

For the perturbed system (1) with $0 < \varepsilon \ll 1$, orbits near the Z-switch fall quickly into a neighborhood of either of the horizontal planes $z = \pm 2$ and stay there most of the time. When that is the case for an orbit, it is approximated by the reduced two-dimensional slow subsystem on $z = \pm 2$. More specifically, near $z = 2$,

$$\dot{x} = -4d(x-a)\,, \quad \dot{y} = -4(y-b)\,,$$

which is obtained by substituting 2 for z in the first two equations of Eq. (1). Note that for $d > 0$, $a > 5$, every trajectory from the left of $x = 4/m - 2$ moves to the right until it reaches the top turning points $x = 4/m - 2$, $z = 2$ of the Z-switch, see Fig. 2(a). It makes a downward turn at the turning points and then behaves approximately like the fast subsystem.

So, the trajectory quickly falls into a neighborhood of the lower branch $z = -2$ of the Z-switch and is approximated by the slow subsystem on $z = -2$:

$$\begin{aligned}
\dot{x} &= 4\left[\alpha(x-2) - \beta y - \alpha(x-2)\frac{(x-2)^2+y^2}{R^2}\right], \\
\dot{y} &= 4\left[\beta(x-2) + \alpha y - \alpha y\frac{(x-2)^2+y^2}{R^2}\right].
\end{aligned}$$

Expressing this equation in terms of the polar coordinates for $(x-2, y)$ yields

$$\dot{r} = 4\alpha r\left(1 - \frac{r^2}{R^2}\right), \quad \dot{\theta} = \beta\,.$$

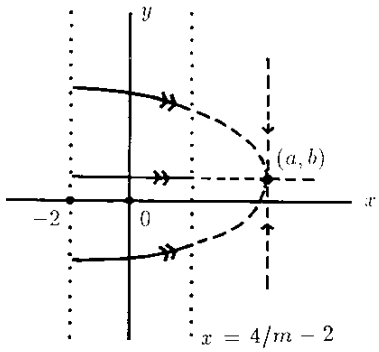

(a)

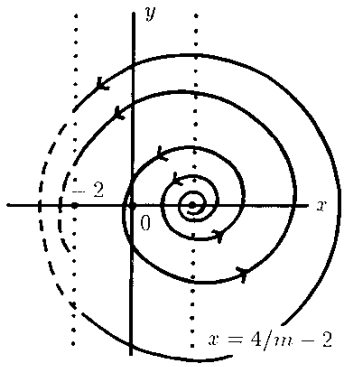

(b)

Fig. 2. The construction of the slow subsystems on (a) $z = 2$ and (b) $z = -2$ respectively. The right dotted line indicates the top turning edge while the left dotted line the bottom turning edge. $m - 1$ and $a > 4/m - 2$ are shown here.

Note that, for $\alpha > 0$, there is a repelling equilibrium point $r = 0$, or $(2, 0)$, and an attracting periodic orbit $r = R$, see Fig. 2(b). Thus, every trajectory originated from the center $(2, 0, -2)$ spirals outwards until it reaches the bottom turning points $x = z = -2$ of the Z-switch. When that happens, it makes an upward turn and behaves like the fast subsystem again, quickly jumping to the upper branch $z = 2$ of the Z-switch. This sets off another cycle of relaxation oscillations.

Due to its normal hyperbolicity (cf. Fenichel [1979]), the center equilibrium $(2, 0, -2)$ persists for small $\varepsilon > 0$ and the eigenvalues of the linearization at the center are approximately $4(\alpha \pm i\beta) + O(\varepsilon)$ and $-16m/\varepsilon - c + O(\varepsilon)$. For $\varepsilon > 0$ small, it is a saddle-focus of the Shil'nikov type. When $\varepsilon = 0$, the top turning edge $x = 4/m - 2$, $z = 2$ is parametrized by m. So, its projection onto the slow branch $z = -2$ can be made to cross the equilibrium point $(2, 0, -2)$ at $m = 1$. Thus, it is plausible to see that m can be chosen as a function m^* of other parameters so that for $m = m^*$ there is a homoclinic orbit for $0 < \varepsilon \ll 1$. This observation together with the fact that the dynamics of Eq. (1) is determined by parameters a, b when it is near the top branch $z = 2$ of the Z-switch and respectively by α, β near the bottom branch $z = -2$ enable us to generate a numerical homoclinic orbit shown in Fig. 3(a). It was a trial-and-error process to fix the parameter values in Fig. 3.

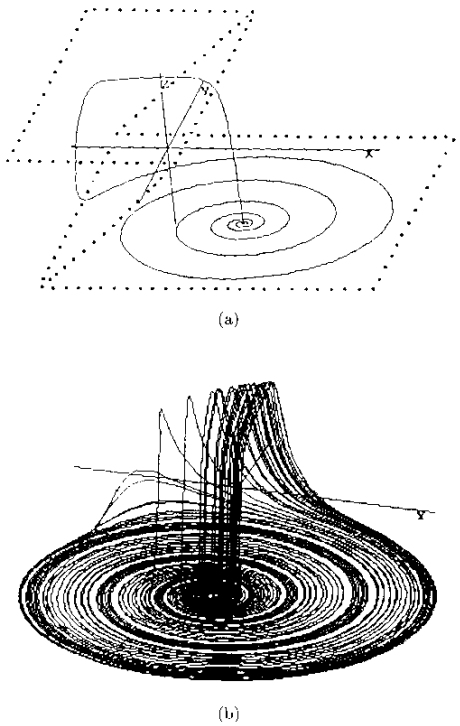

(a)

(b)

Fig. 3. Dotted lines in (a) roughly outline the Z-switch. A Shil'nikov's orbit for Eq. (1) with $a = 7$, $b = 1.435$, $c = 1$, $d = 1.5$, $m = 1.543$, $R = 6$, $\alpha = 0.5$, $\beta = 4$ and $\varepsilon = 0.08$.

Note that a chaotic attractor is evident in Fig. 3(b) and that is mainly due to the nonlinear terms in the slow subsystem on $z = -2$, e.g., the attracting periodic orbit $r = R$. The existence of a Shil'nikov's homoclinic orbit will not be affected by the absence of these nonlinear terms. But it would be not so easy to demonstrate experimentally the existence of a strange attractor as we did here.

We point out that the existence of Shil'nikov's saddle-node homoclinic orbits in other dynamical systems has been considered by, e.g., Arneodo *et al.* [1982] and Gaspard & Nicolis [1983]. The associated strange attractor has also been found in simulations of Chua's circuit, see Chua [1992,1993], Chua *et al.* [1993] and the reference wherein.

2.2. *Double spirals*

Replacing the slow subsystem on the top branch of the Z-switch of Eq. (1) by an oscillatory one yields the following system:

$$
\begin{aligned}
\dot{x} &= (z+2) \\
&\quad \times \left[\lambda(x-k) - \mu y - \lambda(x-k)\frac{(x-k)^2+y^2}{R^2}\right] \\
&\quad + (2-z) \\
&\quad \times \left[\alpha(x-2) - \beta y - \alpha(x-2)\frac{(x-2)^2+y^2}{R^2}\right], \\
\dot{y} &= (z+2) \\
&\quad \times \left[\mu(x-k) + \lambda y - \lambda y\frac{(x-k)^2+y^2}{R^2}\right] \\
&\quad + (2-z)\left[\beta(x-2) + \alpha y - \alpha y\frac{(x-2)^2+y^2}{R^2}\right], \\
\varepsilon\dot{z} &= (4-z^2)[z+2-m(x+2)] - \varepsilon c z\,.
\end{aligned}
\tag{2}
$$

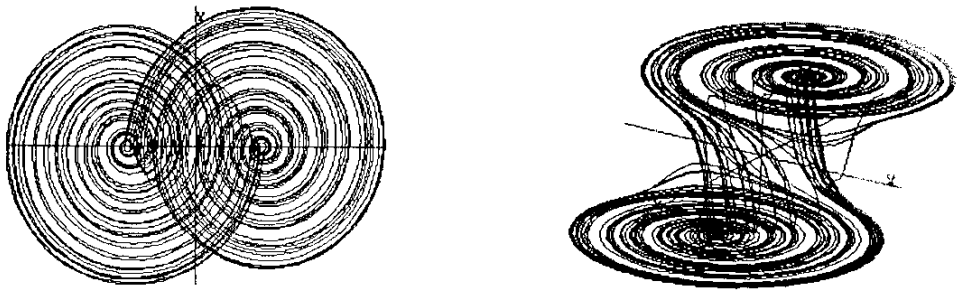

(a) (b)

Fig. 4. A strange attractor for Eq. (2) with $a = 7$, $b = 1.435$, $c = 1$, $m = 1.543$, $k = -3.4$, $R = 6$, $\alpha = 0.5$, $\beta = 4$, $\lambda = 0.5$, $\mu = 4$ and $\varepsilon = 0.08$. (a) The attractor projected on the xy-plane; (b) a three-dimension view of the attractor.

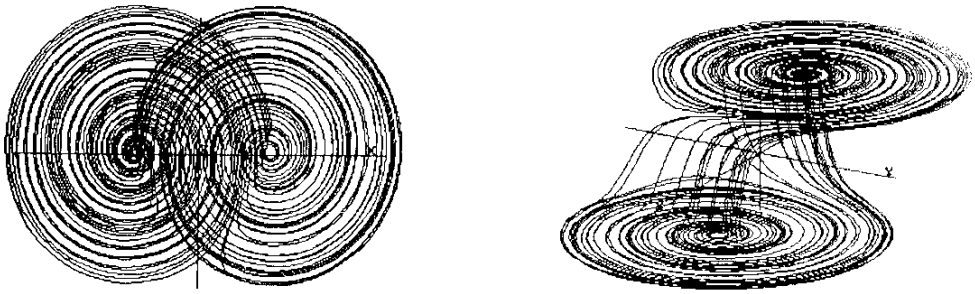

(a) (b)

Fig. 5. Generated for Eq. (2) with the same parameter values as in Fig. 4 except that $k = -3.3$, $\mu = -4$. (a) The attractor projected on the xy-plane; (b) a three-dimension view of the attractor.

where $\lambda > 0, \mu$ and $k < -2$ are new parameters. Figures 4 and 5 correspond to the cases of $\mu > 0$ and $\mu < 0$ respectively. In the former case, orbits on both the top and bottom branches of the Z-switch spiral in the same counterclockwise direction while in the latter case they do so in opposite directions.

We remark that the co-directional-spiral attractor has also been observed in the global unfolding of Chua's circuit, see Chua [1993] and Chua *et al.* [1993].

2.3. *Twisted homoclinic orbit*

Roughly speaking, a system having such an orbit satisfies that the unstable (or stable) manifold twists like a Möbius band. On the other hand, the manifold around a nontwisted homoclinic orbit looks like a cylindrical band. The following system exhibits the bifurcation from one twisting type to the other:

$$\begin{aligned}
\dot{x} &= (2 - z)a(x - 2) + (z + 2) \\
&\quad \times [\alpha(x - x_0) + \beta(y - y_0)], \\
\dot{y} &= (2 - z)[d(b - a)(x - 2)/4 + by] + (z + 2) \\
&\quad \times [-\beta(x - x_0) + \alpha(y - y_0)], \\
\varepsilon\dot{z} &= (4 - z^2)[z + 2 - m(x + 2)] - \varepsilon\mu z.
\end{aligned} \tag{5}$$

The reduced slow systems on the top and bottom branches of the Z-switch are heuristically illustrated in Fig. 6 with the first being represented by dashed curves. It can be directly checked that the reduced slow system on the bottom

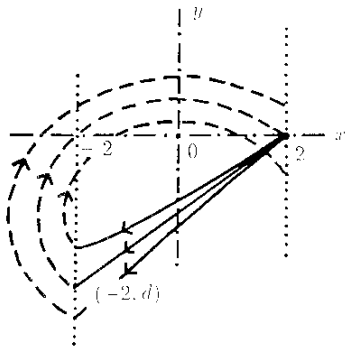

(a)

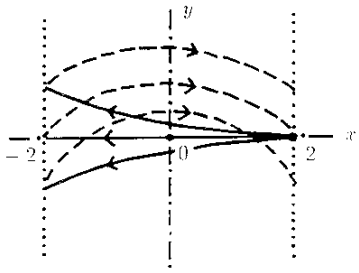

(b)

Fig. 6. The right and left dotted lines in each diagram indicate the top and bottom turning edges respectively. The dashed curves represent the phase portraits for the reduced slow subsystems on the top branch of the Z-switch. (a) A twisted case; (b) a nontwisted case.

branch is

$$\dot{x} = 4a(x-2)\,, \quad \dot{y} = d(b-a)(x-2) + 4by\,,$$

which satisfies the condition that the eigenvalues for the linearization at the only equilibrium point $(2, 0)$ are $4a, 4b$ and the corresponding eigenvectors are $\langle 4, -d\rangle$ and $\langle 0, 1\rangle$ respectively. The parameter d is used to represent the intersection of the (straight) trajectory from the unstable eigenvector $\langle 4, -d\rangle$ and the bottom turning edge $x = z = -2$. Note that $\langle 4, -d\rangle$ is the principal unstable eigenvector if $a < b$ and the intersection point $(-2, d)$ in this case determines roughly where the upturn of the bottom slow flow takes place. On the top branch, however, the spiral center at (x_0, y_0) is used to either add or subtract twists from the three dimensional structure. In fact, half twists of any even number, say $2n$, can be purposely added around the homoclinic orbit by simply adding n more full spirals to the unstable manifold of (x_0, y_0) on the top slow branch before switching it downwards. This can be done by adjusting the parameter value of β accordingly. As numerically shown in Fig. 7 the unstable manifold of the hyperbolic equilibrium point near $(2, 0, -2)$ is twisted for $d = -3.5$ and nontwisted for $d = -0.2$. Hence, the bifurcation of twist must take place somewhere along a

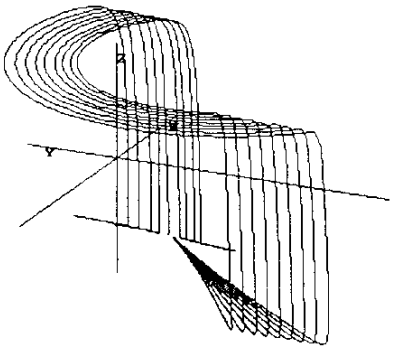

(a)

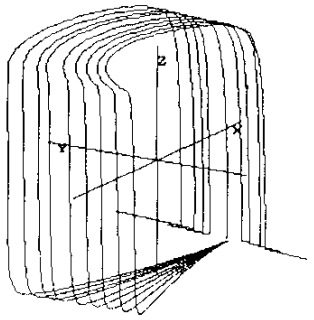

(b)

Fig. 7. (a) A twisted homoclinic orbit for Eq. (3) with $a = 1$, $b = 1.5$, $c = 2$, $m = 1.1845$, $\alpha = 0.01$, $\beta = 5$, $x_0 = -0.1$, $y_0 = -2$, $\varepsilon = 0.01$ and $d = -3.5$; (b) a nontwisted homoclinic orbit for the same parameter values except for $d = -0.2$.

one-parameter family of the system and that family can be parametrized by d. We remark that bifurcations of chaotic dynamics must take place in this example (cf. Deng [1993a]).

2.4. *Relaxation-fold attractor*

Being the same type as Eq. (1), the following system was constructed by Deng [1992] for a relaxation-fold attractor:

$$\begin{aligned}
\dot{x} &= \lambda z(x-a)+(3-z) \\
&\quad \times \left[\alpha(x+0.5)-\beta y-\alpha(x+0.5)\frac{(x+0.5)^2+y^2}{R^2}\right], \\
\dot{y} &= \mu z(y-b)+(3-z) \\
&\quad \times \left[\beta(x+0.5)+\alpha y-\alpha y\frac{(x+0.5)^2+y^2}{R^2}\right], \\
\varepsilon\dot{z} &= z(3-z)(x+z-1.5)+d(x-c)\,.
\end{aligned} \tag{4}$$

The attractor is shown in Fig. 8. The actual folding mechanism is sketched in Fig. 9 in which one bottom trajectory is tangent to the top turning edge when projected onto the bottom branch along the fast flow direction. The resulting fold is referred to as a relaxation fold in Deng [1992]. We remark that the Rössler attractor has a different fold type called branching-reinjection fold. For more details on these two fold types, see Deng [1992].

2.5. *Invariant toroid*

Using a different switch referred to as a toroid-switch, we obtain an attracting invariant toroid in the following system:

$$\begin{aligned}
\dot{x} &= z(\lambda x-\mu y)+(2-z) \\
&\quad \times \left[\alpha x-\beta y-\alpha x\frac{x^2+y^2}{R^2}\right], \\
\dot{y} &= z(\mu x+\lambda y)+(2-z) \\
&\quad \times \left[\beta x+\alpha y-\alpha y\frac{x^2+y^2}{R^2}\right], \\
\varepsilon\dot{z} &= z(2-z)[z+m(x^2+y^2)-h] \\
&\quad -\varepsilon c(z-1)\,,
\end{aligned} \tag{5}$$

where m, h, c, R, $\lambda<0$, μ, $\alpha>0$, β are parameters and ε the singular parameter.

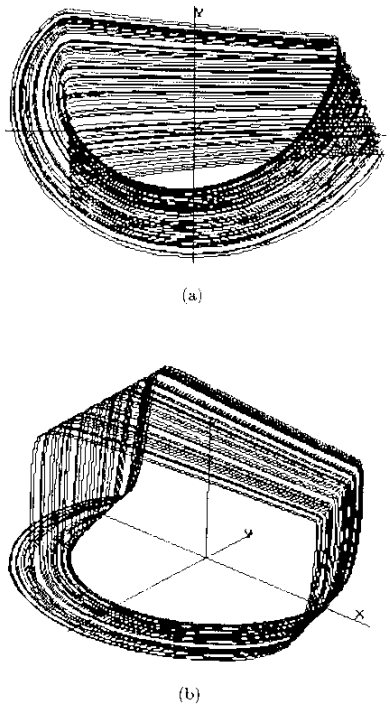

(a) (b)

Fig. 8. A relaxation-fold attractor for Eq. (4) with $a=-0.5$, $b=-0.2$, $c=0.5$, $R=6$, $\alpha=6.2$, $\beta=20$, $\lambda=-1.2$, $\mu=0.7$, $d=0.015$, $\varepsilon=0.006$; (a) projected on the xy-plane, (b) a three-dimensional view.

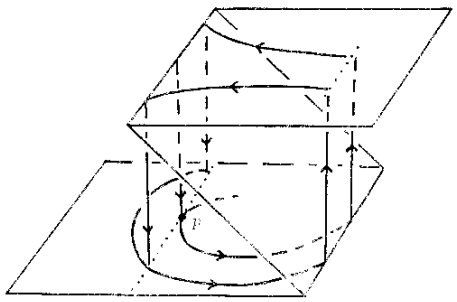

Fig. 9. The dotted line is the projection of the top turning edge onto the bottom slow branch. A relaxation fold takes place when an orbit from the bottom branch is tangent to the projection to the first order.

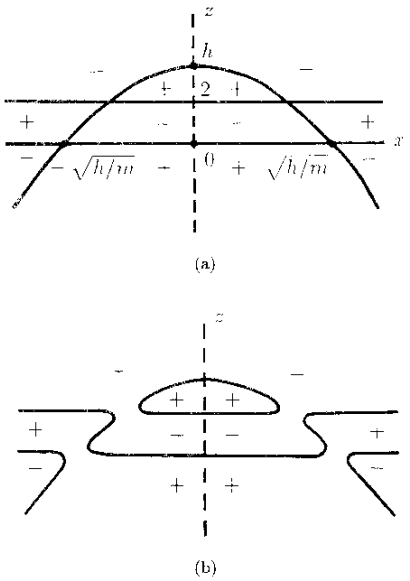

Fig. 10. A cross section of the toroid-switch. ± are the sign for the fast component $\dot{z}$ in the regions partitioned by the nullclines for (a) $\varepsilon = 0$, (b) $\varepsilon > 0$.

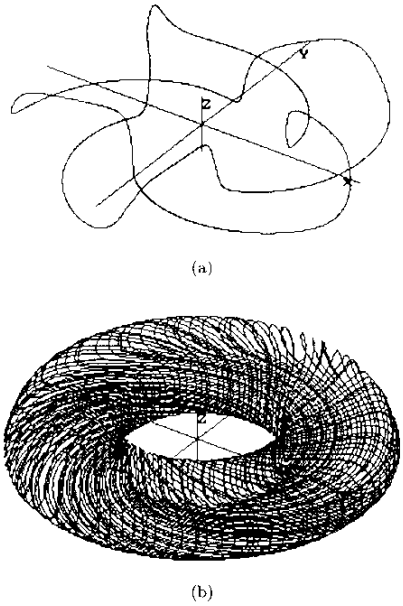

Fig. 11. (a) A knotted periodic orbit for Eq. (5) with $m = 0.1$, $h = 3.6$, $c = 1$, $R = 10$, $\lambda = -4$, $\mu = 2$, $\alpha = 2$, $\beta = 3.0005$. It is attracting on the invariant toroid with rotation vector $(\frac{1}{2}, \frac{2}{5})$. (b) For the same parameter values except for $\mu = -4, \beta = 4$, it appears to be an irrational flow or a periodic orbit with an extremely long period.

Figure 10(a) shows the cross section of the level set $z(2 - z)[z + m(x^2 + y^2) - h] = 0$ on a typical plane containing the z-axis while Fig. 10(b) the cross section of the switch for $\varepsilon > 0$. Note that the switch is rotationally symmetric with respect to the z-axis. More specifically, the top and bottom turning edges are given by the circles $x^2 + y^2 = h/m - 2$ and $x^2 + y^2 = h/m$ respectively with the former interior to the latter when projected onto the xy-plane. The equilibrium points for the reduced slow flows on the top and bottom branches are sink and source respectively so that all bottom trajectories from the center are pushed outward to the upturn circle while all top trajectories from far are pulled inward to the downturn circle. In addition, these two equilibrium points can be made either clockwise or counterclockwise spirals depending on the signs of μ, β. Numerical simulations are shown in Fig. 11.

2.6. *Folded tori*

Note that the reduced slow vector field on the bottom branch of the toroid-switch of Eq. (5) is transverse not only to the bottom turning circle but also to the projection of the top turning circle on the bottom branch. The same is also true for the reduced slow vector field on the top branch. This prevents the system from developing chaos prone folds, see Deng [1992]. Such transversality is a result of many symmetrical and special arrangements in Eq. (5). To name a few, circular spirals are used for both the top and bottom slow flows; both equilibria are aligned on the same z-axis; the top and bottom branches are parallel planes; and the side branch is a rotationally symmetric paraboloid. Chaotic motion emerges if any one of these features is purposely changed.

In the first example that follows, chaos is produced by slightly tilting the top branch of the toroid-switch. This is done by replacing the factor $(2-z)$ in the $\dot{z}$-equation of Eq. (5) by $(2-z)[a(z-2)^2+b]-dx$. Here, b is near 1, d is small, and a is not necessarily

small for being the coefficient of the high order term $(z-2)^3$ when z is near 2. The modified system is

$$\begin{aligned}
\dot{x} &= z(\lambda x - \mu y) + (2-z) \\
&\quad \times \left[\alpha x - \beta y - \alpha x \frac{x^2+y^2}{R^2}\right], \\
\dot{y} &= z(\mu x + \lambda y) + (2-z) \\
&\quad \times \left[\beta x + \alpha y - \alpha y \frac{x^2+y^2}{R^2}\right], \\
\varepsilon \dot{z} &= z[(2-z)[a(z-2)^2 + b] - dx] \\
&\quad \times [z + m(x^2+y^2) - h] - \varepsilon c(z-1),
\end{aligned} \tag{6}$$

where a, b, d are the additional parameters. Figure 12(a) shows a side view of the limiting switch at $\varepsilon = 0$ while Fig. 12(b) is the projection onto the

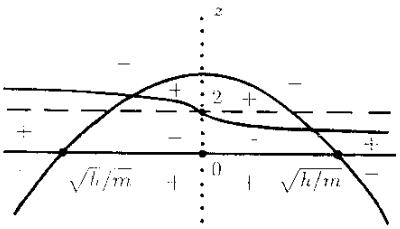

(a)

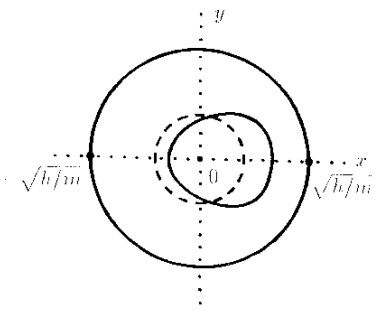

(b)

Fig. 12. (a) The cross section of the perturbed toroid-switch on the xz-plane when $\varepsilon = 0$. (b) The projection of the perturbed switch onto the xy-plane.

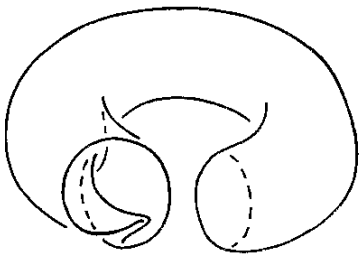

(a)

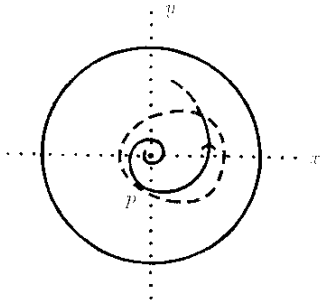

(b)

Fig. 13. In (b), the dashed curve is the projection of the top turning edge. A quadratic type tangency with an orbit on the bottom branch takes place at the relaxation-fold point p.

xy-plane. For comparison, dashed curves are used to indicate the original, unperturbed counterparts. Note that for $b > 0$ the top branch is lifted at one end and lowered at the other end as the inner turning circle distorts and shifts to the right. These changes amount to in effect pinching part of the invariant toroid and folding it back to the surface as illustrated in Fig. 13(a). The folding mechanism is the same relaxation-fold as in Eq. (4) and it is depicted in Fig. 13(b). Numerical simulations are shown in Fig. 14. We remark that simply tilting the top branch will result in the same phenomenon and the cubic nonlinearity, especially when it starts to fold the top branch into a Z-switch for $b < 0$, is made primarily for a different use later.

The next folded toroid example is taken from Deng [1992] in which the circular spiral on the bottom branch of the toroid-switch from Eq. (5) is

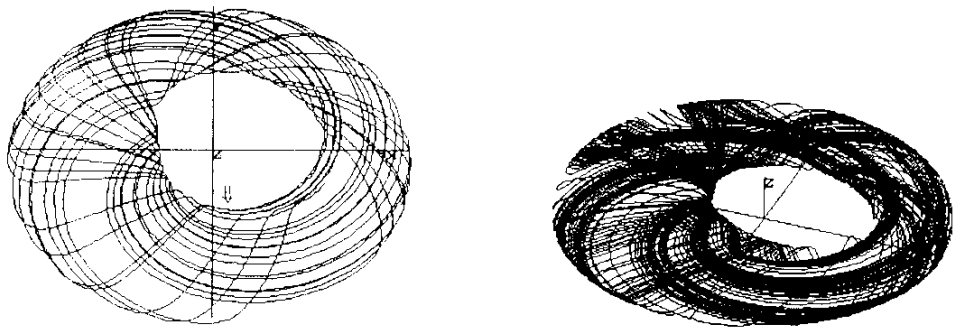

(a) (b)

Fig. 14. A folded toroid attractor for Eq. (6) with $a = 3$, $b = 0.8$, $c = 1$, $d = 0.1$, $m = 0.05$, $h = 3.312$, $R = 10$, $\lambda = -2$, $\mu = 1$, $\alpha = 2.8$, $\beta = 5$ and $\varepsilon = 0.1$. (a) The projection of the attractor onto the xy-plane. The arrow marks the place where the relaxation fold takes place. (b) A three-dimensional view of the attractor.

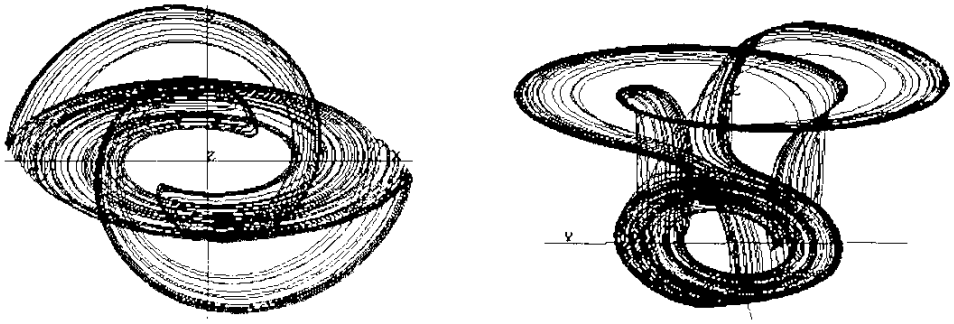

(a) (b)

Fig. 15. A folded toroid attractor for Eq. (7) with $a = 5$, $c = 1$, $h = 2.76$, $m = 0.26$, $R = 5$, $\lambda = -2$, $\mu = -10$, $\alpha = 1$, $\beta = 4$, $\varepsilon = 0.03$. (a) The projection onto the xy-plane; (b) a three-dimensional view of the attractor.

replaced by an elliptic one. The constructed system is as follows:

$$\begin{aligned}
\dot{x} &= z(\lambda x - \mu y) + (2 - z) \\
&\quad \times \left[\alpha x - a\beta y - \alpha x \frac{x^2 + y^2}{R^2}\right], \\
\dot{y} &= z(\mu x + \lambda y) + (2 - z) \\
&\quad \times \left[\beta x + \alpha y - \alpha y \frac{x^2 + y^2}{R^2}\right], \\
\varepsilon \dot{z} &= z(2 - z)[z + m(x^2 + y^2) - h] \\
&\quad - \varepsilon c(z - 1),
\end{aligned} \tag{7}$$

where the new parameter a is used to distort the circular spiral into an elliptic spiral. A strange attractor is shown in Fig. 15.

Strange tori attractors have also been demonstrated in Rössler [1979] as well as in Chua's circuit. [Chua, 1993 and Chua *et al.*, 1993.]

3. Combination Switches

3.1. *ZZ-switch*

Recall from Eq. (1) that the Shil'nikov saddle-focus homoclinic orbit lies entirely on one branch of the stable manifold of the equilibrium point. Making

the other branch of the stable manifold into another homoclinic orbit yields the following system:

$$\begin{aligned}
\dot{x} &= -z(z+2)(x-x_1) - z(z-2)(x-x_2) \\
&\quad + (4-z^2)\left[\alpha x - \beta y - \alpha x\frac{x^2+y^2}{R^2}\right], \\
\dot{y} &= -z(z+2)(y-y_1) - z(z-2)(y-y_2) \\
&\quad + (4-z^2)\left[\beta x + \alpha y - \alpha y\frac{x^2+y^2}{R^2}\right], \\
\varepsilon\dot{z} &= z(4-z^2)[z-2a(x/3+1)] \\
&\quad \times [z-2b(x/3-1)] - \varepsilon c(z+x),
\end{aligned} \tag{8}$$

where a, b, c, R, α, β, x_1, y_1, x_2, y_2 are parameters and ε the singular parameter. In this example, we put one Z-switch on the top of another Z-switch to get a ZZ-switch, which is illustrated in Fig. 16. In order to direct the reduced slow flows to various turning edges of the three branches we simply use saddle points in the top and bottom branches ($z = \pm 2$) and an outward spiral center in the middle ($z = 0$). Figure 17(a) shows what appears to be our intended two homoclinic orbits and Fig. 17(b) the attractor. We point out that symmetry appears in this system in many ways only because of its

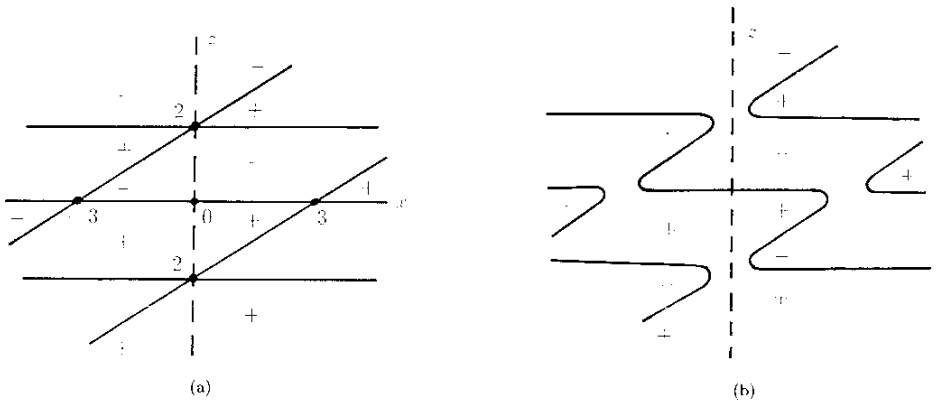

(a) (b)

Fig. 16. The construction of a ZZ-switch. $\pm$ are the sign for the fast component $\dot{z}$ in the regions partitioned by the nullclines for (a) $\varepsilon = 0$, (b) $\varepsilon > 0$.

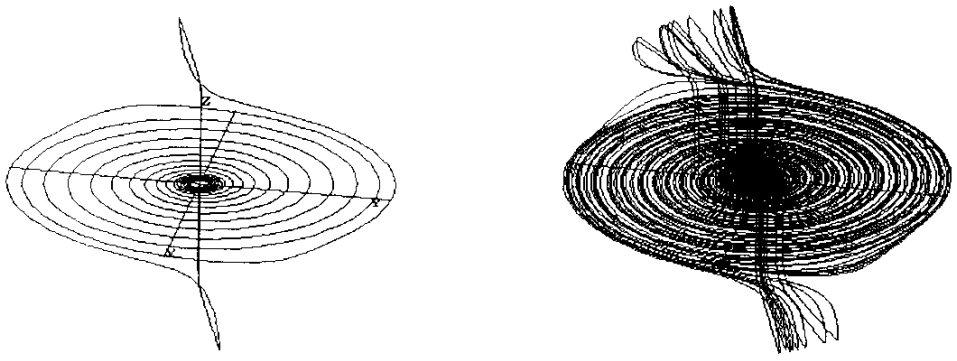

(a) (b)

Fig. 17. (a) Two Shil'nikov's orbits of the same equilibrium point for Eq. (8) with $a = 1.15$, $b = 1.15$, $c = 1$, $R = 4$, $\alpha = 0.5$, $\beta = 6$, $x_1 = -x_2 = 1.5$, $y_1 = -y_2 = 0.5$ and $\varepsilon = 0.1$. (b) The attractor generated by following one orbit.

simplicity. It does not play any critical role in this example.

We remark that the type of attractors shown in Fig. 17(b) has also been found in the global unfolding of Chua's circuit, see Chua [1993] and Chua *et al.* [1993].

Next, we couple three oscillators together by a ZZ-switch and obtain this system:

$$\begin{aligned} \dot{x} &= z(z+4)f_1 + (16-z^2)f_2 + z(z-4)f_3\,, \\ \dot{y} &= z(z+4)g_1 + (16-z^2)g_2 + z(z-4)g_3\,, \\ \varepsilon\dot{z} &= z(16-z^2)[z-a(x-c)] \\ &\quad \times [z-b(x+4)] - \varepsilon(z+x)\,, \end{aligned} \tag{9}$$

where

$$f_1 = \phi(x, y, 0.5, 3, -4, 0)\,, \quad f_2 = \phi(x, y, 0.5, 2.0, 0)\,,$$

$$f_3 = \phi(x, y, 0.5, 3, 4.0)\,, \quad g_1 = \psi(x, y, 0.5, 3, -4, 0)\,,$$

$$g_2 = \psi(x, y, 0.5, 2, 0, 0)\,, \quad g_3 = \psi(x, y, 0.5, 3, 4, 0)\,,$$

and

$$\phi(x, y, \alpha, \beta, x_0, y_0) = \alpha(x - x_0) - \beta(y - y_0) - \alpha(x - x_0)\frac{(x-x_0)^2 + (y-y_0)^2}{R^2}\,,$$

$$\psi(x, y, \alpha, \beta, x_0, y_0) = \beta(x - x_0) + \alpha(y - y_0) - \alpha(y - y_0)\frac{(x-x_0)^2 + (y-y_0)^2}{R^2}\,.$$

Note that as shown in Fig. 18(b), the top oscillator can also be connected to the bottom one directly whereas in Fig. 18(a) only adjacent oscillators can be switched to each other. One can also purposely shut off the top or bottom oscillator by disconnecting the top or the bottom branch from the switch. This will results in an instantaneous change in size for the attractor.

3.2. *Toroid-Z-switch*

In this example, we simply put a Z-switch on the top of a toroid-switch. As mentioned earlier, such coupling is easy to do by choosing $b < 0$ in Eq. (6). Figure 19 shows two side views of the resulting switch at the singular limit $\varepsilon = 0$. Figure 20 shows a curl like attractor and Fig. 21 two different views of another attractor.

Note that $\varepsilon = 0.5$ in this example may be regarded as far away from the singular value $\varepsilon = 0$. If the system were presented in a context different than singular perturbations, it would be difficult to trace the origin back to relaxation oscillations.

3.3. *Toroid-toroid-switch*

In this example, we will construct an invariant double toroid. To do so, we need to attach two toroid-switches together side by side. Key elements include this polynomial function:

$$H(x, y) = \frac{(x-y)^4}{64} - \frac{x^2 - y^2}{2} + \frac{(x+y)^2}{4}\,,$$

and the equation

$$\dot{x} = x(x^2 - 8)/16\,.$$

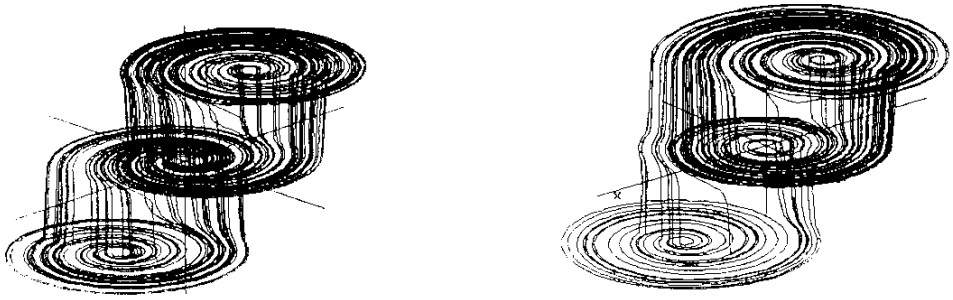

(a) (b)

Fig. 18. (a) A triple spiral attractor for Eq. (9) with $a = b = 1$, $c = 4$, $\varepsilon = 0.09$ and f_i, g_i as stated in the text. (b) Another triple spiral attractor for Eq. (9) with $a = 2/3$, $b = 3/4$, $c = 6$, $\varepsilon = 0.075$, $f_1 = \phi(x, y, 0.5, 3.5, -4, 0)$, $f_2 = \phi(x, y, 0.5, 2, 0, 0)$, $f_3 = \phi(x, y, 0.5, 3, 6, 0)$, $g_1 = \psi(x, y, 0.5, 3.5, -4, 0)$, $g_2 = \psi(x, y, 0.5, 3, 6, 0)$ and $g_3 = \psi(x, y, 0.5, 2, 0, 0)$.

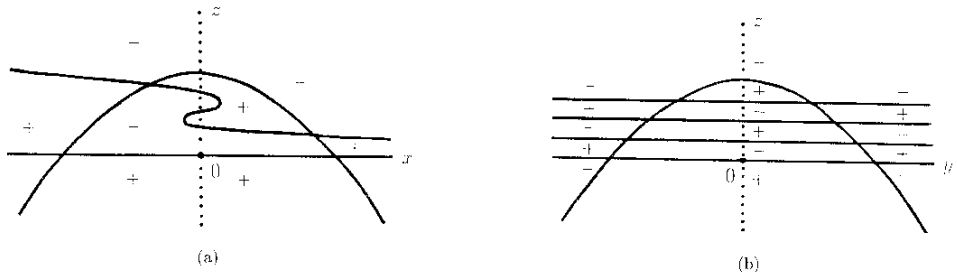

(a) (b)

Fig. 19. For the perturbed toroid-switch of Eq. (6), the top branch folds into a Z-switch when $b < 0$. This gives rise to a combined toroid-Z-switch. (a) The cross section of the combined switch on the xz-plane at $\varepsilon = 0$. (b) The cross section with yz-plane.

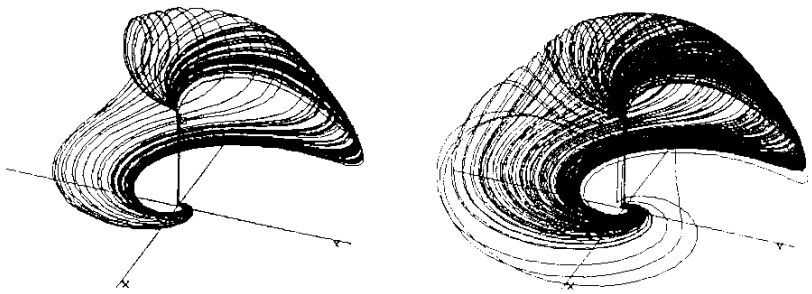

(a) (b)

Fig. 20. A curl like attractor for Eq. (6) with $a = 2$, $b = -0.08$, $c = 1$, $d = 1$, $m = 0.26$, $h = 2.76$, $R = 5$, $\lambda = -2$, $\mu = 1$, $\alpha = 3$, $\beta = -4$, $\varepsilon = 0.5$. (b) The same attractor with a longer integration time.

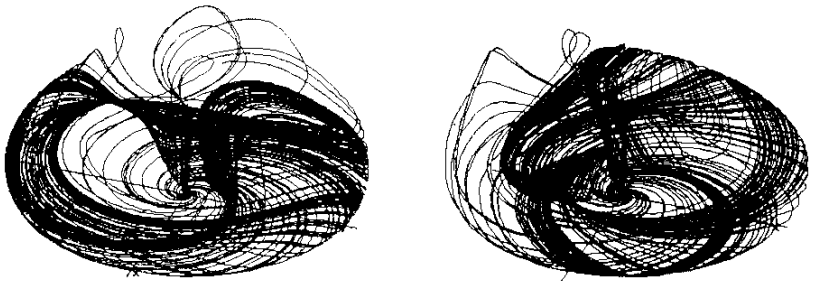

(a) (b)

Fig. 21. Generated with the same parameter values as in Fig. 20 except for $a = 3$, $b = 0.3$, $\beta = -5$. (a) looks like a (desert) storm whereas (b) looks like a calligraphic but nonexisting Chinese character.

It is easy to verify that the function $z = 1 - H(x, y)$ has one saddle point $(0, 0)$ and two maximum points $(\pm 2\sqrt{2}, 0)$ with the same maximum value $z = 2$. It is also easy to see that the $\dot{x}$-equation has one saddle at $x = 0$ and two sources at $x = \pm 2\sqrt{2}$. The model system is

$$\begin{aligned}
\dot{x} &= a(1.5 - z)x(x^2 - 8)/16 + bz[\alpha(\alpha x + \beta y) \\
&\quad \times [8 - (\alpha x + \beta y)^2]/16 - \beta(\beta x - \alpha y)], \\
\dot{y} &= a(1.5 - z)y + bz[\beta(\alpha x + \beta y) \\
&\quad \times [8 - (\alpha x + \beta y)^2]/16 + \alpha(\beta x - \alpha y)], \\
\varepsilon \dot{z} &= z(1.5 - z)[z - 1 + H(x, y)] + \varepsilon(3/4 - z),
\end{aligned} \tag{10}$$

where parameters a, b satisfy $\alpha = \cos\theta$, $\beta = \sin\theta$.

The switch's cross section on the xz-plane for $\varepsilon = 0$ is shown in Fig. 22(a). The outer closed curve in Fig. 22(b) is the level set $1 - H(x, y) = 0$. It forms the bottom turning edge which switches the bottom slow flow upwards. Similarly, the two inner closed curves are the level set $1 - H(x, y) = 1.5$. They form the top turning edge, switching the top slow flow downwards.

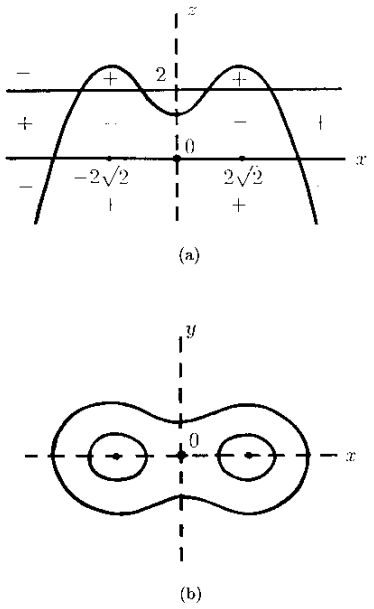

Fig. 22. (a) The cross section of the combined toroid-toroid-switch with the xz-plane when $\varepsilon = 0$. $\pm$ are the sign for the fast component $\dot{z}$ in the regions partitioned by the nullclines. The curved nullcline is the cross section of the surface $z = 1 - H(x, y)$ with the plane. (b) The bottom and top turning edges that correspond to the level curves $z = 0$, $z = 1.5$ of $z = 1 - H(x, y)$ respectively.

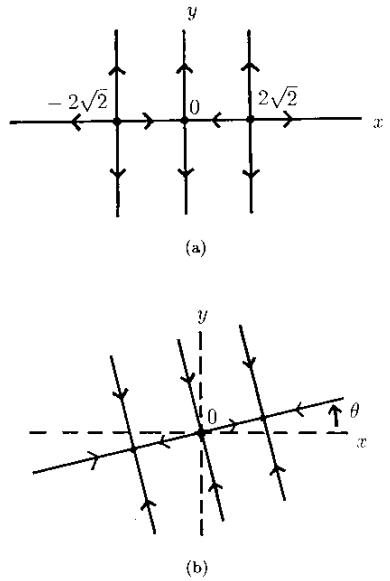

Fig. 23. (a) The phase portrait for the slow subsystem on the bottom branch $z = 0$ of the combined switch. (b) The phase portrait for the slow subsystem on the top branch $z = 1.5$ of the combined switch.

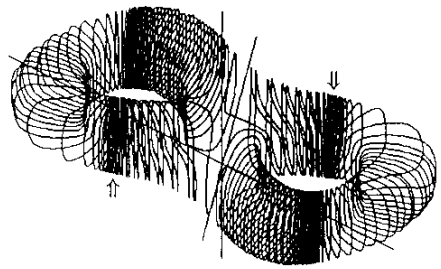

Fig. 24. The invariant double toroid for Eq. (10) with $a = b = 1$, $\theta = 0.08$ and $\varepsilon = 0.06$. Arrows mark the attracting periodic orbits. The two saddle points lie near the origin and $(0, 0, 1.5)$ respectively.

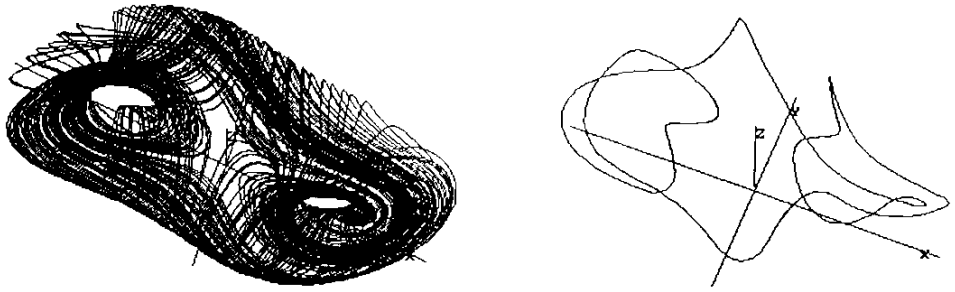

(a) (b)

Fig. 25. (a) A strange attractor for Eq. (11) with $a = 15$, $b = 3$, $c = 0.5$, $\theta = 0$ and $\varepsilon = 0.03$. (b) A knotted attracting periodic orbit for $a = 10$, $b = 1$, $c = 2$, $\theta = 0.1745$ and $\varepsilon = 0.06$.

As shown in Fig. 23(a), the reduced bottom system is

$$\dot{x} = 1.5ax(x^2 - 8)/16\,, \quad \dot{y} = 1.5ay$$

which has one saddle at the origin and two sources at $(\pm 2\sqrt{2}, 0)$. And, the reduced top vector field is obtained by reversing the reduced bottom vector field in time, followed by a θ degree rotation, see Fig. 23(b). Figure 24 shows an invariant double toroid on which there are two saddle points, two attracting and two repelling periodic orbits, and the rest are heteroclinic orbits.

Similar to Eqs. (6, 7) on folded invariant tori, it is also easy to introduce chaotic motions in this case. Presented here is one of such perturbed systems. Replacing the reduced bottom flow by oscillations produced by this perturbed Hamiltonian system $\dot{x} = -\partial H/\partial y$, $\dot{y} = \partial H/\partial x + cy$, we have

$$\begin{aligned}
\dot{x} &= a(1.5 - z)\left(-\frac{\partial H}{\partial y}\right) + bz[\alpha(\alpha x + \beta y) \\
&\quad \times [8 - (\alpha x + \beta y)^2]/16 - \beta(\beta x - \alpha y)]\,, \\
\dot{y} &= a(1.5 - z)\left(\frac{\partial H}{\partial x} + cy\right) + bz[\beta(\alpha x + \beta y) \\
&\quad \times [8 - (\alpha x + \beta y)^2]/16 + \alpha(\beta x - \alpha y)]\,, \\
\varepsilon\dot{z} &= z(1.5 - z)[z - 1 + H(x, y)] + \varepsilon(3/4 - z)\,.
\end{aligned} \tag{11}$$

Note that Fig. 22(b) can also be regarded as three periodic orbits on two typical level surfaces of the Hamiltonian H for the unperturbed system $\dot{x} = -\partial H/\partial y$, $\dot{y} = \partial H/\partial x$. The perturbation term cy is purposely used to break up all such closed orbits and make them spiral outwards when modulated onto the bottom branch. Figure 25(a) shows a chaotic attractor and Fig. 25(b) a knotted attracting periodic orbit.

4. A Three-Time-Scale Switch

The method presented above can also be used progressively to construct systems as building blocks for higher dimensional systems which in turn are used as building blocks for even higher dimensional systems, and so on. The following example taken from Deng, [1993b] is used to illustrate this point.

In contrast to all previous examples, this example has a two-dimensional fast subsystem and a one-dimensional slow subsystem. Moreover, instead of through a turning point, it switches the fast flow to the slow flow through a homoclinic orbit.

To be precise, the system satisfies the following properties. When parametrized by the slow variable x, the fast subsystem in y, z has a branch of stable equilibrium points that terminates at a saddle-node point. It also has a branch of attracting periodic orbits that terminates at a homoclinic orbit, see Fig. 26(a). For the perturbed system, any orbit that starts near the attracting equilibrium branch moves to the right until it reaches the saddle-node turning point. In a neighborhood of that turning point, it makes an upward turn and quickly jumps into a neighborhood of the periodic orbit branch. Then, it winds around the periodic orbit branch leftwards until it reaches the separatrix homoclinic orbit. After passing the homoclinic orbit, the orbit falls into the other side of the unstable

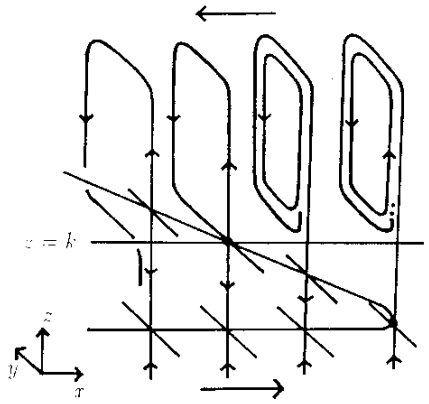

(a)

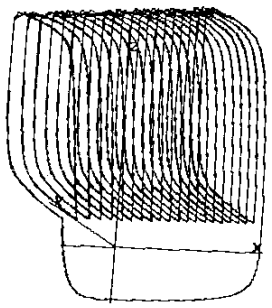

(b)

Fig. 26. (a) A depiction of Rinzel's geometrical mechanism for bursting oscillations. It represents the phase portraits of the fast subsystem parametrized by the slow variable x. The nullcline for the $\dot{x}$-equation of Eq. (12) is $z = k$ which is depicted here for $k \approx 0$. The two horizontal arrows indicate the directions in which the x-variable moves when the z-variable is either above or below the plane of nullcline $z = k$. (b) A bursting-oscillation orbit for Eq. (12) with $a = 6$, $b = 0.8$, $c = 3$, $d = 0.6$, $e = 0.05$, $f = 0.55$, $g = 1$, $h = -1$, $n = 1.1$, $y_0 = 0.8$, $z_0 = 1.9$, $z_1 = -0.4$, $\varepsilon_1 = 0.021$, $\varepsilon_2 = 0.0065$ and $k = 0.1512$.

manifold and is attracted to the attracting equilibrium branch again, setting off another round of so-called bursting-oscillations. This two-time-scale mechanism was first used by Rinzel [1985] as a qualitative model for the glucose-induced bursting-oscillations for the membrane potential of pancreatic β-cells. It has been demonstrated in Terman [1992] that the dynamics generated by this geometrical mechanism must be chaotic and it can also give rise to complicated bifurcations as observed in many numerical simulations, see the references in Deng [1993b].

In Deng [1993b], we first constructed the fast subsystem in variables y, z as another singularly perturbed system, treating variable x as a parameter. We then coupled the fast and slow subsystems together by turning x into a slowly drifting variable. The resulting system is given as follows:

$$\begin{aligned}
\dot{x} &= a(k - z)\,, \\
\varepsilon_2\varepsilon_1\dot{y} &= -by(y - y_0)[y_0(z - z_0) + nz_0y] \\
&\quad - \varepsilon_1 c\left(y - \frac{y_0}{2}\right), \qquad (12) \\
\varepsilon_2\dot{z} &= d(y_0 - y)[f(z - z_1)(z - hx) + e] - gy\,,
\end{aligned}$$

where a, b, c, d, e, f, g, h, k, n are parameters and ε_1, ε_2 are singular parameters. The differentiation here is taken with respect to a time variable, say t. Casting this system in terms of the slow time-scale $\tau = \varepsilon_2 t$, $\varepsilon_2 > 0$ with respect to the singular variable ε_2 results in the following system:

$$\begin{aligned}
x' &= \varepsilon_2 a(k - z)\,, \\
\varepsilon_1 y' &= -by(y - y_0)[y_0(z - z_0) + nz_0y] \\
&\quad - \varepsilon_1 c\left(y - \frac{y_0}{2}\right), \qquad (13) \\
z' &= d(y_0 - y)\left[f(z - z_1)(z - hx) + e\right] - gy\,.
\end{aligned}$$

The fast subsystem with respect to ε_2 is obtained by setting $\varepsilon_2 = 0$ in Eq. (13). The resulting system below is two-dimensional with the x-variable as a parameter:

$$\begin{aligned}
\varepsilon_1 y' &= -by(y - y_0)[y_0(z - z_0) + nz_0y] \\
&\quad - \varepsilon_1 c\left(y - \frac{y_0}{2}\right), \qquad (14) \\
z' &= d(y_0 - y)[f(z - z_1)(z - hx) + e] - gy\,.
\end{aligned}$$

This system is again singularly perturbed in ε_1 and variable y is the faster of the fast variables. The Z-switch is sketched in Fig. 27(a) for $\varepsilon_1 > 0$. It consists of the roots of the cubic polynomial $-by(y - y_0)[y_0(z - z_0) + nz_0y] - \varepsilon_1 c(y - \frac{y_0}{2})$ in y for $\varepsilon_1 > 0$.

The slow subsystem of Eq. (14) is obtained by setting $\varepsilon_1 = 0$. It is a one-dimensional system

$$z' = d(y_0 - y)[f(z - z_1)(z - hx) + e] - gy$$

sitting on the singular surface $-by(y - y_0)[y_0(z - z_0) + nz_0y] = 0$. When reduced to the singular branch $y = 0$, the slow subsystem is

$$z' = dy_0[f(z - z_1)(z - hx) + e].$$

For $e = 0$, there are two branches of equilibrium points: $z = z_1 \approx -0.4$ and $z = hx$ with $h \approx -1$, as illustrated in Fig. 27(b). Being the roots of the quadratic polynomial $f(z - z_1)(z - hx) + e$ in z, the two branches bifurcate and reorganize themselves into two new branches for $0 < e \ll 1$ as illustrated in Fig. 27(c). Note that each knee point of the new branches becomes a saddle-node bifurcation point with x as the bifurcation parameter. The slow subsystem of Eq. (14) on the other singular branch $y = y_0$ is simply $\dot{z} = -gy_0$ with $g = 1$, a flow with constant velocity $-gy_0 < 0$. The parametrized fast phase portrait is shown in Fig. 26(a). Now, coupling the slow system $\dot{x} = a(k - z)$ with Eq. (14) gives rise to Eq. (12).

Intuitively, the resulting vector field of Eq. (12) slowly drifts to the right near the steady state branch $y \approx 0$, $z \approx z_1$ because $\dot{x} = a(k - z) > 0$ for $k > z_1$. In contrast, the trains of rapid oscillations in variables y, z move slowly to the left because $\dot{x} = a(k - z) < 0$. The fast transition from the steady state branch to the branch of periodic oscillations takes place near the knee point $x \approx -z_1 = 0.4$, $y \approx 0$, $z \approx z_1$. The reversed fast transition takes

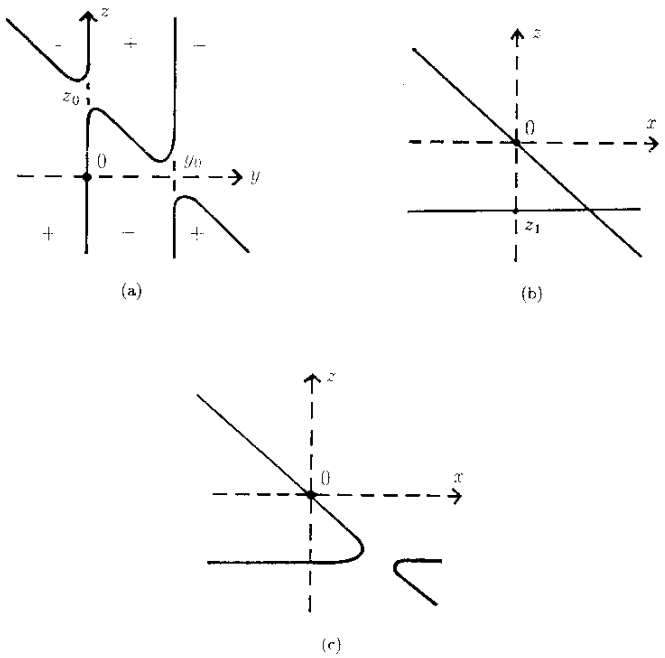

Fig. 27. (a) Solid curves are nullclines for the faster y'-equation of the fast system (14) with $\varepsilon_1 > 0$. The Z-switch lies on its side. $\pm$ are the sign for y' in the regions partitioned by the nullclines. The two branches other than the Z-switch are outside the region of interest. (b, c) By treating x as a parameter, the solid curves consist of equilibrium points of the slow subsystem of Eq. (14) on the branch of singular manifold $y = 0$. They correspond to $e = 0$, $0 < e \ll 1$ respectively. The left most knee point is the saddle-node bifurcation point required by Rinzel's geometrical mechanism and the other knee is outside the region of interest.

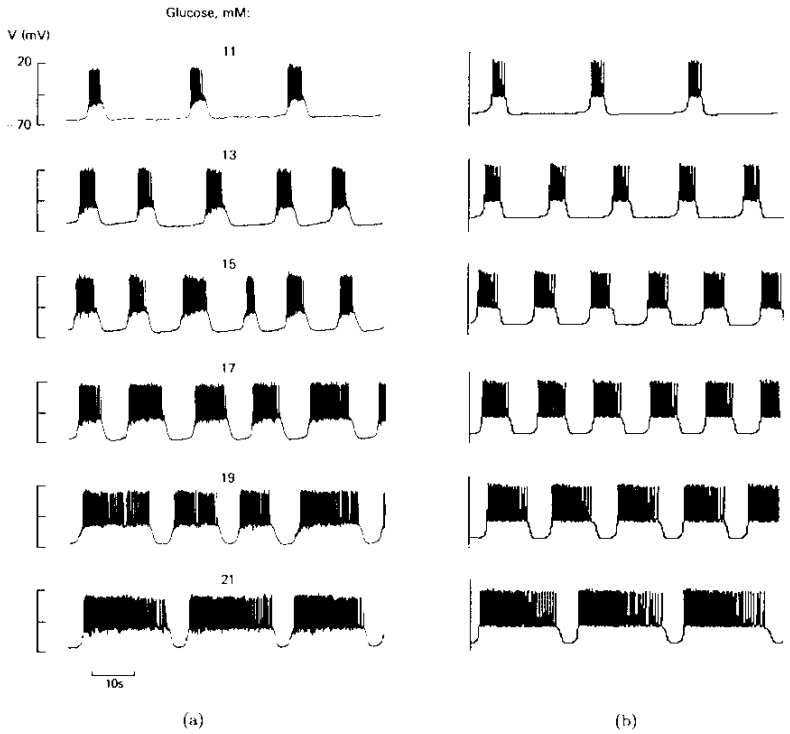

Fig. 28. (a) Membrane potential record obtained from a single β-cell with a 6-min. exposure to each glucose concentration. (b) The z-variable time-series for Eq. (12) with the same parameter values as in Fig. 26(b) and $k = -0.222, -0.0976, 0.0268, 0.1512, 0.2756, 0.4$ respectively from top down. Calibrating the graded glucose concentrations, the k values are also spaced equally with the step size 0.1244.

place near $x \approx 0$, $y \approx 0$, $z \approx 0$. In fact, the existence of a homoclinic orbit occurs at some parameter value of $k \approx 0$ and the only equilibrium point for the perturbed system is near $z = k$, $y \approx 0$, $x = z/h$. This realizes Rinzel's two-time-scale mechanism for bursting-oscillations in two successive steps of singular perturbations and the order of time scales is $x < z < y$.

A numerical orbit of Eq. (12) is shown in Fig. 26(b). Figure 28 compares the time-series of the z-variable with the glucose-induced bursting-oscillations for the membrane potentials in pancreatic β-cells. The numerical simulations match the experimental data very well, see Deng [1993b] for more details.

5. Conclusion

We have demonstrated a systematic, practical, and simple way to construct homoclinic orbits and chaotic attractors. The method is based on homotopy coupling of fast subsystems of the Rössler type and slow subsystems which satisfy certain geometric specifications. This method can also be used progressively to construct systems as building blocks for higher dimensional systems which in turn are used as building blocks for even higher dimensional systems, and so on. Systems constructed in this way are simple, robust, and ideal for experimental and theoretical manipulations. In this practical sense, these models may be regarded as the origins

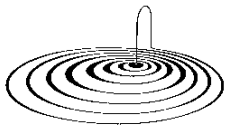

Fig. 29. The preprint series logo for CDSNS.

as well as normal forms for the dynamical structures they are designed to portrait. Moreover, the construction of such a model may provide us with a better understanding about the geometry of the natural system the model describes.

Acknowledgments

The author is grateful for the hospitality of the Center for Dynamical Systems and Nonlinear Studies at Georgia Tech. during his visit in the summer of 1990. It was the institute's preprint series logo (Fig. 29) that the author originally wanted to mimic mathematically. The author also thanks Steve Dumbar for many stimulating discussions and his expertise in numerical simulations. All numerical orbits were generated by PhasePlane, a numerical package created by Ermentrout [1988] who has made an otherwise painstaking numerical probing much more tolerable and sometimes enjoyable. He also wants to thank the authors of Sherman *et al.* [1990] for allowing him to use Fig. 28(a).

References

Arneodo, A., Coullet, P. & Tresser, C. [1982] "Oscillators with chaotic behavior: An illustration of a theorem by Shil'nikov," *J. Stat. Phys.* **27**, 171–182.

Chua, L.O. [1992] "The genesis of Chua's circuit," *AEÜ* **46**, 250–257.

Chua, L.O. [1993] "Global unfolding of Chua's circuit," *IEICE Trans. Fundamentals* **E76-A**, 704–734.

Chua, L.O., Wu, C.W., Huang, A. & Zhong G.-Q. [1993] "A universal circuit for studying and generating chaos—part I: routes to chaos; part II: strange attractors," *IEEE Trans. Circuit and Systems* **40**, 732–761.

Deng, B. [1992] "Folding at the genesis of chaos," to appear in *Proceedings of the First World Congress of Nonlinear Analysts.*

Deng, B. [1993a] "Homoclinic twisting bifurcations and cusp horseshoe maps," *J. D. D. E.* **5**, 417–467.

Deng, B. [1993b] "A mathematical model that mimics the bursting oscillations in pancreatic β-cells," *Math. Biosciences* **119**(2), 241–250.

Ermentrout, B. [1988] *PhasePlane, 3.0* (Brooks/Cole Publishing Company)

Fenichel, N. [1979] "Geometric singular perturbation theory for ordinary differential equations," *J. D. E.* **73**, 309–353.

Gaspard, P. & Nicolis, J. [1983] "What can we learn from homoclinic orbits in chaotic systems?" *J. Stat. Phys.* **31**, 499–518.

Rinzel, J. [1985] "Bursting oscillations in an excitable membrane model," in *Ordinary and Partial Differential Equations*, eds. Sleeman, B. D. & Jarvis, R. J. (Springer-Verlag, New York) pp. 304–316.

Rössler, O. E. [1976] "Chaotic behavior in simple reaction systems," *Z. Naturforsch* **31A**, 259–264.

Rössler, O. E. [1979] "Continuous chaos—four prototype equations," in *Bifurcation Theory and Applications in Scientific Disciplines*, eds. Gurel, O. & Rössler, O. E. *Annals of the New York Academy of Science*, **316**, pp. 376–392.

Sherman, A., Carroll, P., Santos, R. M. & Atwater, I. [1990] "Glucose dose response of pancreatic β-cells: experimental and theoretical results" in *Transduction in Biological Systems*, eds. Hidalgo, C., Bacigalupo, J., Jaimovich, E. & Vergara, J. (Plenum Publishing Co.) pp. 123–141.

Shilnikov, L. P. [1970] "A contribution to the problem of the structure of an extended neighborhood of a rough equilibrium state of saddle-focus type," *Math. USSR-Sb.* **10**, 91–102.

Terman, D. [1992] "The transition from bursting to continuous spiking in excitable membrane models," *J. Nonlinear Science* **2**, 135–182.